Design of a Collapse-Mode CMUT With an Embossed Membrane for Improving Output Pressure

Yuanyu Yu, *Student Member, IEEE*, Sio Hang Pun, *Member, IEEE*, Peng Un Mak, *Senior Member, IEEE*, Ching-Hsiang Cheng, *Member, IEEE*, Jiujiang Wang, *Student Member, IEEE*, Pui-In Mak, *Senior Member, IEEE*, and Mang I Vai, *Senior Member, IEEE*

***Abstract*— Capacitive micromachined ultrasonic transducers (CMUTs) have emerged as a competitive alternative to piezoelectric ultrasonic transducers, especially in medical ultrasound imaging and therapeutic ultrasound applications, which require high output pressure. However, as compared with piezoelectric ultrasonic transducers, the output pressure capability of CMUTs remains to be improved. In this paper, a novel structure is proposed by forming an embossed vibrating membrane on a CMUT cell operating in the collapse mode to increase the maximum output pressure. By using a beam model in undamped conditions and finite-element analysis simulations, the proposed embossed structure showed improvement on the maximum output pressure of the CMUT cell when the embossed pattern was placed on the estimated location of the peak deflection. As compared with a uniform membrane CMUT cell worked in the collapse mode, the proposed CMUT cell can yield the maximum output pressure by 51.1% and 88.1% enhancement with a single embossed pattern made of Si_3N_4 and nickel, respectively. The maximum output pressures were improved by 34.9% (a single Si_3N_4 embossed pattern) and 46.7% (a single nickel embossed pattern) with the uniform membrane when the center frequencies of both original and embossed CMUT designs were similar.**

***Index Terms*— Capacitive micromachined ultrasonic transducer (CMUT), embossed membrane, output pressure.**

Manuscript received January 11, 2016; accepted April 11, 2016. Date of publication April 15, 2016; date of current version June 1, 2016. This work was supported by the Research Committee of the University of Macau under Grant MRG014/MPU/2014/FST, Grant MYRG076(Y1-L2)-FST12-MPU, Grant MYRG079(Y1-L2)-FST12-VMI, Grant MYRG103(Y1-L3)-FST13-VMI, and Grant MYRG2014-00010-AMSV, and by the Science and Technology Development Fund of Macau (FDCT) under Grant 024/2009/A1, Grant 087/2012/A3, and Grant 047/2013/A2.

Y. Yu, J. Wang, P.-I. Mak, and M. I Vai are with the State Key Laboratory of Analog and Mixed-Signal VLSI, University of Macau, Macau 999078, China, and also with the Department of Electrical and Computer Engineering, Faculty of Science and Technology, University of Macau, Macau 999078, China (e-mail: yuyuanyu@gmail.com; tswangjade@gmail.com; pimak@umac.mo; fstmiv@umac.mo).

S. H. Pun is with the State Key Laboratory of Analog and Mixed-Signal VLSI, University of Macau, Macau 999078, China (e-mail: lodgepun@umac.mo).

P. U. Mak is with the Department of Electrical and Computer Engineering, Faculty of Science and Technology, University of Macau, Macau 999078, China (e-mail: fstpum@umac.mo).

C.-H. Cheng is with the State Key Laboratory of Analog and Mixed-Signal VLSI, University of Macau, Macau 999078, China, and also with the Department of Industrial and Systems Engineering, The Hong Kong Polytechnic University, Hong Kong, China (e-mail: ching-hsiang.cheng@polyu.edu.hk).

Digital Object Identifier 10.1109/TUFFC.2016.2554612

I. Introduction

Ultrasound imaging, because of its low cost and little ionization, has become a popular diagnostic tool in medical imaging for more than 60 years [1]. Based on the fundamental vibrating principles, such as piezoelectric and electrostatics, an ultrasonic transducer converts electrical signals into ultrasound waves; and vice versa, generates electrical signals corresponding to the bounced back ultrasound echoes. By the sophisticated hardware and reconstruction algorithm from the received echoes, high-quality images of internal organs can be obtained noninvasively. Being the fore part of an ultrasound imaging system, the performance (for instance, efficiency, bandwidth, and so on) of the ultrasonic transducer has great influence on the quality of the acquired image.

Capacitive micromachined ultrasonic transducers (CMUTs) have been considered as an alternative to piezoelectric transducers. Although the idea of this electrostatic transducer for ultrasound was old, the early versions of CMUTs have not been demonstrated until in the later 1980s [2] and early 1990s [3] because of the limitations of the fabrication technology. With the advancements of microelectromechanical system technology, a CMUT can sustain electric fields higher than 10^6 V/cm [4] inside the gap and its electromechanical coupling efficiency is comparable with general lead–zirconate–titanate (PZT) transducers. As compared with the PZT transducers, CMUTs own advantages, such as better matched acoustic impedance to human body, wider bandwidth, higher operating frequency, easier to realize highly integrated array with interconnections to front-end electronics, and so on, which make CMUTs suitable for medical imaging [4] and therapeutic ultrasound applications [5]. In recent years, a pulse-echo-phased 1-D linear CMUT array with 16-element [6], a 1-D linear CMUT array with 128-element for B-mode ultrasound imaging [4], and a 2-D CMUT array with 8×16-element for volumetric imaging [7] were fabricated and reported.

Even though the CMUTs offer advantages over PZT transducers in medical ultrasonic imaging, to increase the output pressure in transmission, which means deeper penetration and better image quality in clinical application of ultrasound, remains one of the pursuits of the CMUT design. In an early experiment of real-time *in vivo* imaging, the loop gain of CMUT arrays in the pulse-echo experiment was 10 dB lower than that of PZT arrays [8]. In CMUT design, the gap

0885-3010 © 2016 IEEE. Personal use is permitted, but republication/redistribution requires IEEE permission.
See http://www.ieee.org/publications_standards/publications/rights/index.html for more information.

height can affect the performance in both transmission and reception. For a conventional CMUT, a large gap is desired in transmission for better output pressure. However, for a CMUT in reception, a small gap means more sensitivity.

To circumvent this tradeoff in a conventional CMUT design, several CMUT operating modes, such as collapse mode [9]–[12], collapse-snapback mode [13], and deep-collapse mode [14], were proposed. A collapse-mode CMUT offers better performance in both transmission and reception than a conventional CMUT, because the electric field inside the cavity is higher [11]. Besides operating in various modes for improvements, the output pressure can also be increased by altering the CMUT structure with a center mass on the membrane to increase the membrane displacement in transmission [15]–[17].

In this paper, aiming at increasing the output pressure of CMUTs, a novel CMUT structure for the collapse-mode operation is proposed. This structure includes an annular embossed pattern on the vibrating membrane, so that the maximum vibrating amplitude is increased, and therefore, the output pressure is boosted, without increasing the gap height of the device and the bias voltages in operation. In the new structure, the embossed pattern was similar to [15]–[17] that placed a mass on the membrane to obtain improvement. For those CMUTs worked in the conventional mode, the mass was generally placed at the geometrical center of the membrane. However, in this paper, it is found that placing the embossed pattern at the vibrating center of the vibrating structure obtains the best performance and the geometrical center happens to coincide with the vibrating center in the conventional mode. It is also found that placing the embossed pattern at the vibrating center has the minimum effect to the membrane stiffness. Thus, we believe that the embossed pattern should be placed at the vibrating center of the membrane, when it is not overlapping with the geometrical center in the collapse mode. In the following, the methodology of forming the embossed membrane and the analysis of finding the vibrating center are given in Section II. Section III introduces the finite-element analysis (FEA) method of placing an embossed pattern on different positions. The simulation results and discussion of this structure can be found in Section IV, and finally, Section V concludes this paper.

II. Methodologies

In this section, the detail of the proposed CMUT design is discussed. Fig. 1 shows the 3-D outlook and 2-D axisymmetric (respected to its center axis) cross-sectional view of the proposed design. In this configuration, the CMUT is designed to work in the collapse mode. In this mode, the center portion of the membrane is attached to the bottom of the cavity and the membrane can be divided into the contact portion and the vibrating portion, which are circular and annular, respectively.

During operation, a DC bias voltage, which is higher than the pull-in voltage, is applied to the membrane in order to drive the device into the collapse mode. Then, an AC voltage is applied and the vibrating portion generates the corresponding acoustic waves. This mechanism possesses two distinct advantages for enhancing output pressure. First, a high electromechanical coupling coefficient is obtained because of the reduced gap height [10]. Second, the ratio of the average membrane displacement to the peak membrane displacement is higher than that in the conventional mode CMUT, leading to more output pressure [12].

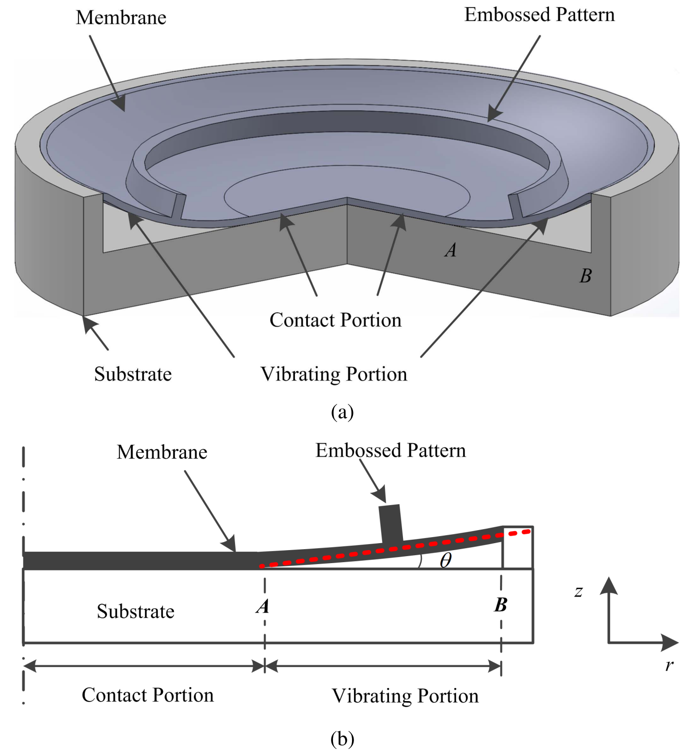

Fig. 1. (a) 3-D outlook view and (b) 2-D axisymmetric cross-sectional view of the proposed collapse-mode CMUT with an embossed membrane.

To further improve the maximum membrane displacement, an embossed pattern, which is equivalent to alter the mass and the inertia of the device vibrating structure, is placed at the location of the maximum displacement of the vibrating membrane. The effects of the embossed pattern, which is added on the vibrating portion, can be explained by a beam model, as shown in Fig. 2. In this model, the vibrating portion of the membrane is simplified as a simply supported uniform beam. Its mass per unit length is defined as $\bar{m}$ and the flexural rigidity is EI. The embossed structure is represented by an additional mass M on the beam. For the vibrating portion of the membrane, the electrostatic force is not uniformly distributed due to the inclined structure respect to the substrate. As a result, a linear varying distributed load p', as defined by (1), is used to approximate this nonuniform pressure exerted on the beam that behaves in a linear elastic manner and follows Hooke's law whenever the deflection is small:

$$p'(x) = \frac{p_o}{L}(L - x') \tag{1}$$

where p_o is the maximum pressure at the edge of the contact portion of the membrane.

To demonstrate the slant membrane, an angle between the beam and horizontal is set as θ, as shown in Fig. 2(a). As for the collapse-mode CMUTs in both experiments and simulations [9]–[12], [18], [19], θ was very small. Assuming F is the external load applied vertically, the normal

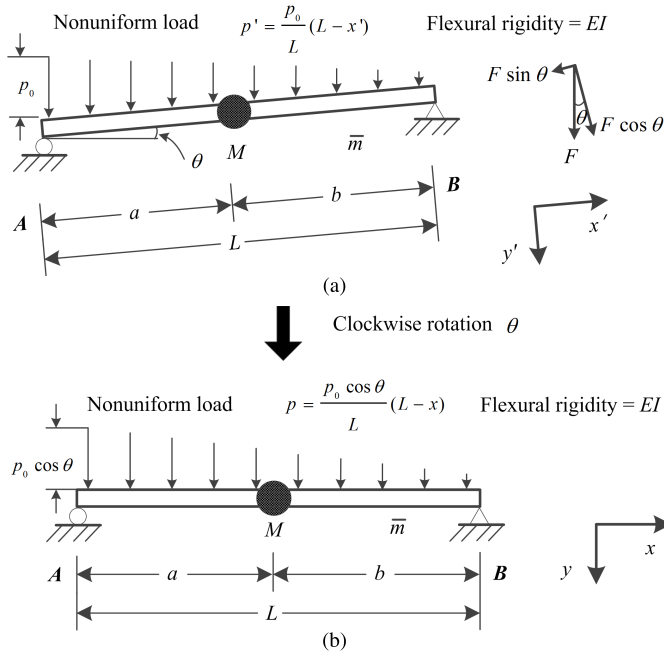

Fig. 2. Simply supported beam model with an additional mass. (a) Inclined simply supported beam model with an additional mass (in coordinate system x'-y'). (b) The simply supported beam model with an additional mass after transformation (in coordinate system x-y).

component of load to the beam becomes $F\cos\theta$. In this paper, only the normal components are concerned, and the coordinate system $x' - y'$ is then converted into the coordinate system $x - y$ by clockwise rotating θ, as shown in Fig. 2(b). The following analysis is based on the coordinate system $x - y$. All the magnitudes of loads analyzed in this coordinate system are modulated by multiplying a factor of $\cos\theta$. The linear varying distributed load p' is then modulated as p (2) to represent the electrostatic force

$$p(x) = \frac{p_0}{L}\cos\theta(L - x). \tag{2}$$

In the current design of CMUT, the first resonance frequency is concerned and the model is analyzed as a single-degree-of-freedom (SDOF) system without damping. A direct method of calculating the strain energy using deflected shapes caused by applied loads is employed here [20]. In the model, the defection of the beam ψ can be calculated by the superposition of the deformations caused by multiple loads, namely, the gravity load, the distributed load, and the load by the additional mass on the beam

$$\psi(x) = y_1(x) + y_2(x) + y_3(x) \tag{3}$$

where

$$y_1(x) = \frac{\bar{m}gx}{24EI}\cos\theta(L^3 - 2Lx^2 + x^3) \tag{4}$$

$$y_2(x) = \frac{p_o(L-x)}{360LEI}\cos\theta[7L^4 - 10L^2(L-x)^2 + 3(L-x)^4] \tag{5}$$

$$y_3(x) = \begin{cases} \frac{Mgbx}{6LEI}\cos\theta(L^2 - x^2 - b^2), & 0 \le x \le a \\ \frac{Mgb}{6LEI}\cos\theta\left[\frac{L}{b}(x-a)^3 + x(L^2 - b^2) - x^3\right] & \\ & a < x \le L \end{cases} \tag{6}$$

a and b show the distances of the mass M measured from points A and B, respectively.

In (3)–(6), $y_1(x)$ is the deflection caused by the beam gravity, $y_2(x)$ is the deflection produced by the distributed load, and $y_3(x)$ is the deflection caused by the additional mass [21].

The location of M is determined by a and b in (6). As for a conventional CMUT, an additional mass is generally located at the geometrical center of the membrane to improve the output pressure [15]–[17]. On the contrary, in the collapse mode, the maximum deflection position $X_{\max}$ is not coincided with the geometrical center of the membrane due to the nonuniform electrostatic force on the vibrating portion. Theoretically, all the considered loads in the system contribute to $X_{\max}$. However, the embossed pattern is smaller than the membrane, and the electrostatic force is dominant in the collapse mode. Thus, $X_{\max}$ can be approximated by the position of peak deflection caused by the electrostatic force, represented by p. According to [21], for the deflection profile of $y_2(x)$ caused by p, the maximum deflection of the beam occurs at

$$X_{\max} \approx 0.481L. \tag{7}$$

From (3), when a beam undergoes free vibration, the maximum strain energy $U_{\max_emb}$ stored in the beam with an additional mass at $X_{\max}$ can be expressed as

$$U_{\max_emb} = \frac{1}{2}g\cos\theta\left\{\bar{m}\left[\int_0^L y_1(x)dx + \int_0^L y_3(x)dx\right] + M\left[y_1(X_{\max}) + y_3(X_{\max})\right]\right\}. \tag{8}$$

If no additional mass on the beam, which can be considered as a special case representing the uniform membrane CMUT in the collapse mode, the terms associated with the additional mass M in (8) are eliminated, and the maximum strain energy $U_{\max_uni}$ stored in this beam is given as

$$U_{\max_uni} = \frac{1}{2}\bar{m}g\cos\theta\left[\int_0^L y_1(x)dx\right]. \tag{9}$$

In addition, in accordance with [20], the strain energy is equal to the elastic potential energy stored in the system. Therefore, the maximum elastic potential energy $V_{\max}$ in this SDOF system is given by (10) and is equal to the maximum strain energy of the beam

$$V_{\max} = \frac{1}{2}kA^2 = U_{\max} \tag{10}$$

where k is the global spring constant of the elastic beam and A is the maximum amplitude of the system in vibration, which is equivalent to the beam displacement in the model. Compared with (8) and (9), an additional mass at $X_{\max}$ gives higher strain energy as stated in

$$U_{\max_emb} - U_{\max_uni} = \frac{1}{2}g\cos\theta\left\{\bar{m}\int_0^L y_3(x)dx + M[y_1(X_{\max}) + y_3(X_{\max})]\right\}. \tag{11}$$

From (10), the maximum displacement of the beam is proportional to the maximum strain energy, and the additional

mass located at X_{max} has a slight modification to k. Therefore, the extra energy stored in the beam with a mass located at X_{max} results in an increased vibration amplitude, which is equivalent to a larger membrane displacement of the CMUT. According to [13], [15], and [22], a larger membrane displacement leads to a higher output pressure.

This beam model can also be used to analyze the influences to the undamped natural resonance frequency by the additional mass located at X_{max}. Since the system is energy conservative with no external force interference, the total energy, including kinetic and strain energy, remains constant, and the maximum kinetic energy T_{max_emb} is equal to the maximum strain energy U_{max_emb}, as stated in

$$T_{max_emb} = U_{max_emb} = \text{constant}. \tag{12}$$

For a beam with an additional mass located at X_{max}, U_{max_emb} and T_{max_emb} are calculated by using (8) and (13), respectively

$$T_{max_emb} = \frac{1}{2}\omega_{emb}^2 \left\{ \int_0^L \bar{m}[y_1(x) + y_3(x)]^2 dx + M[y_1(X_{max}) + y_3(X_{max})]^2 \right\} \tag{13}$$

where ω_{emb} is the natural resonance frequency of the system. By using (12), the expression for ω_{emb} is given by

$$\omega_{emb}^2 \approx \frac{EI}{ML^3} \frac{37.5\alpha^2 + 117\alpha + 93.5}{0.384\alpha^3 + 1.97\alpha^2 + 3.38\alpha + 1.94} \tag{14}$$

where $\alpha = (m/M)$, and $m = \bar{m}L$ is the mass of the beam.

For no additional mass case, α tends to infinity and the limit of (14) gives ω_{uni}, which is the natural resonance frequency of a uniform beam without any additional mass, as follows:

$$\omega_{uni}^2 = \lim_{\alpha\to\infty} \omega_{emb}^2 \approx 97.7\frac{EI}{mL^3}. \tag{15}$$

Then, by comparing ω_{emb} and ω_{uni}, (16) reveals that the natural resonance frequency is decreased due to the additional mass located at X_{max}

$$\frac{\omega_{uni}^2}{\omega_{emb}^2} \approx \frac{\alpha^3 + 5.12\alpha^2 + 8.80\alpha + 5.07}{\alpha^3 + 3.12\alpha^2 + 2.49\alpha} > 1. \tag{16}$$

In summary, the model shows that for the proposed collapse-mode CMUT with an embossed membrane, the maximum output pressure can be increased with an embossed pattern at the peak deflection position on the vibrating membrane. At the same time, the embossed pattern lowers the resonance frequency of the system.

III. Finite-Element Analysis

To investigate the behavior of the proposed collapse-mode CMUT cell with an embossed pattern on the membrane, the FEA method was used. The FEA models were developed by the commercial software COMSOL Multiphysics 4.4 (COMSOL, Inc., Stockholm, Sweden).

In order to research on the effects caused by the embossed membrane, two single CMUT cells, which have a uniform membrane [Fig. 3(a)] and an embossed membrane [Fig. 3(b)], were built in a 2-D axisymmetric system surrounding with a hemispheric water medium for efficient simulation.

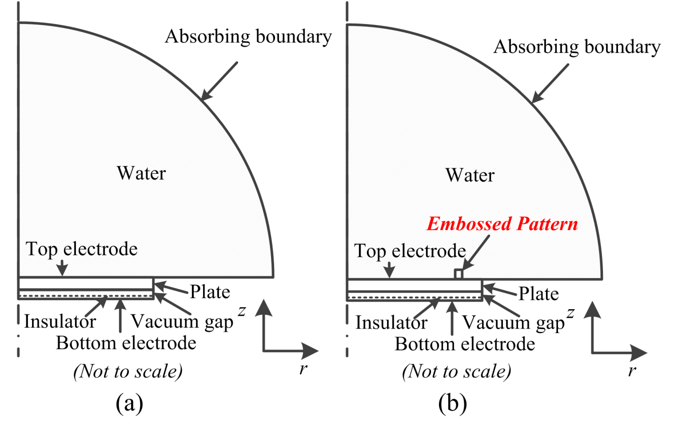

Fig. 3. Illustration of CMUT models in COMSOL. (a) Uniform membrane CMUT model. (b) Embossed membrane CMUT model.

TABLE I
DIMENSION OF THE COLLAPSE-MODE CMUT IN FEA SIMULATION

Model dimension	(μm)
Plate radius	25
Plate thickness	0.6
Gap height	0.4
Insulator thickness	0.11
Water medium radius	150
Embossed pattern width	1.0
Embossed pattern height	2.0

Two physics in COMSOL, including electromechanics (*emi*) and pressure acoustic (*acpr*), were coupled in these models. The *emi* governed all the components of the CMUT cell, namely, plate, vacuum gap, insulator, and electrodes. For the water medium, both *emi* and *acpr* were applied. The outer surfaces of the water medium were set as an absorbing boundary to eliminate the acoustic wave reflection.

The membranes of the CMUTs, which were represented by the plates in Fig. 3, had the material properties of plasma-enhanced chemical vapor deposition (PECVD) Si_3N_4 with their rims fixed. The top electrodes covered full area over the plate and the bottom electrodes located underneath the insulator layer. Both the electrodes were considered as infinitely thin for simplification. The rectangular block on the plate, shown in Fig. 3(b), was used to represent the embossed pattern upon the membrane and it was made of PECVD Si_3N_4 as well. Between the vacuum gaps and the bottom electrodes in both models, there were thin SiO_2 layers acting as insulator layers to prevent electrical short circuit. In addition, 1-atm constant pressure was applied to each plate to represent the load over the vacuum gap. The dimensions of models are shown in Table I. In the simulations, *emi* was coupled with *acpr* by setting the acoustic load per unit area on the top of plate, and the normal acceleration was set as the boundary condition in *acpr*. The previous boundary condition applied with the loads from the *acpr* domain to the *emi* domain and the latter boundary condition set the plate vibration as the acoustic source in the *acpr* domain. The maximum mesh size in *acpr* domain was limited to one-eighth of the wavelength of the operating frequency. The material properties used in FEA are given in Table II [14], [18], [19].

TABLE II
MATERIAL PARAMETERS USED IN FEA SIMULATION

Material parameters	
Young's modulus of Si_3N_4	110 GPa
Poisson's ratio of Si_3N_4	0.27
Dielectric permittivity of Si_3N_4	5.4
Density of Si_3N_4	3100 kg/m^3
Dielectric permittivity of SiO_2	3.7

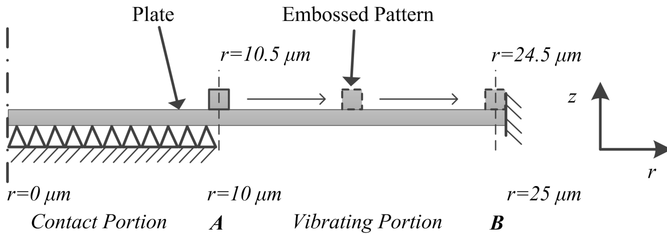

Fig. 4. 2-D axisymmetric view of the embossed pattern located on the membrane.

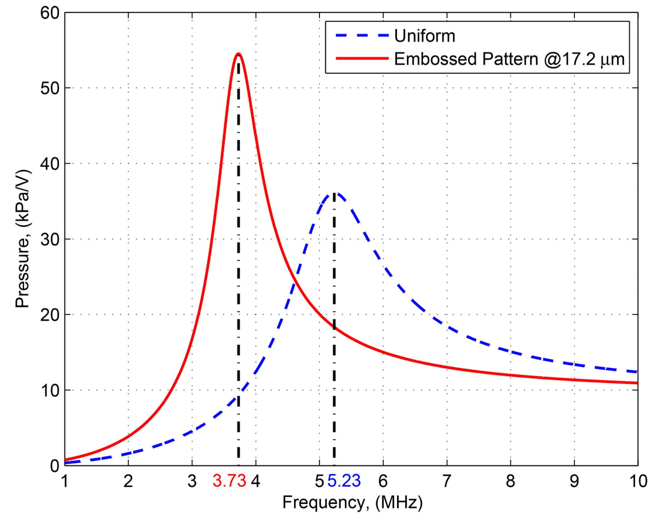

Fig. 5. Output pressure comparison between the uniform membrane and the embossed membrane CMUT in the collapse mode.

In order to calculate the pressure over different frequencies, the prestressed analysis was applied. First, a stationary study was used to calculate the plate deformation under a certain DC bias voltage. The contact between the plate and the insulator was handled by a penalty or barrier method [23]. To avoid divergence, a DC bias voltage was applied with a sweeping method in this stationary study. Then, an AC voltage was applied for harmonic perturbation analysis to obtain the output pressure over different frequencies. In this paper, the output pressure was calculated by averaging the pressure along the interface between the plate and water medium, which was similar to the methods introduced in [12] and [24].

For both models, the DC bias voltage was set to 130 V, which was higher than pull-in voltage, and the AC voltage was set as 1 V. The contact radius for the uniform membrane model was approximately 10 μm.

In the following, the effects of the embossed pattern to the performance of the CMUT are presented. The simulations were performed for various positions of the embossed pattern, and the results of the uniform membrane model were acquired as a reference. Fig. 4 shows the position of the embossed pattern on the plate before collapse. Since the contact radius of the membrane was 10 μm, the simulations were performed for the embossed pattern centered from $r = 10.5$ μm to $r = 24.5$ μm with 1 μm step. According to (7), an extra simulation was performed for the embossed pattern centered at $r = 17.2$ μm corresponding to the estimated location of the peak deflection on the plate.

IV. RESULTS AND DISCUSSION

With the FEA models introduced in Section III, the behavior of placing the embossed pattern can be simulated and investigated. The material properties of PECVD Si3N4 in the FEA models were adopted from [14], [18], and [19]; while [14] includes both FEA simulation and experiment results, [18] and [19] give the collapse-mode CMUT models. In this section, the output pressure improvement, center frequency shift, and further possible improvement regarding to the proposed design are discussed.

A. Output Pressure Improvement

Fig. 5 shows the average output pressures over the surface of the membrane for the embossed pattern membrane model and the uniform membrane model over a range of operating frequencies. In Fig. 5, red solid line indicates the performance of the embossed pattern centered at $r = 17.2$ μm and the blue dashed line represents the uniform membrane model. For the embossed pattern model, the maximum average output pressure was 54.5 kPa/V occurred at 3.73 MHz. In comparison with the uniform membrane model, which was 36.1 kPa/V at 5.23 MHz, the embossed pattern model achieved 51.1% improvement in the maximum average output pressure.

The dynamic displacement profiles of the collapsed CMUTs with and without an embossed pattern at 17.2 μm excited by 1 V AC voltage under 130 V DC bias voltage were shown in Fig. 6. The displacement profiles were evaluated at the center frequency of the uniform membrane CMUT (5.23 MHz) and the embossed membrane CMUT (3.73 MHz), respectively. The maximum displacement was boosted in the embossed pattern membrane case by nearly 9 nm. The results qualitatively agreed with the behavior, which the embossed pattern membrane gives increased vibration amplitude but lower center frequency, as explained by the beam model in Section II.

To further evaluate the performance of the new structure, the pressure-bandwidth product [25] was introduced as a figure of merit for evaluation. From Fig. 5, the pressure-bandwidth products of the embossed membrane CMUT and the uniform membrane CMUT were 36.2 and 51.4 kPa MHz, respectively. However, as the center frequency of the embossed membrane CMUT was reduced, the thickness of the membranes were changed to maintain the similar center frequencies to ensure a fair comparison. For the embossed pattern located at 17.2 μm, the membrane center frequency can be tuned

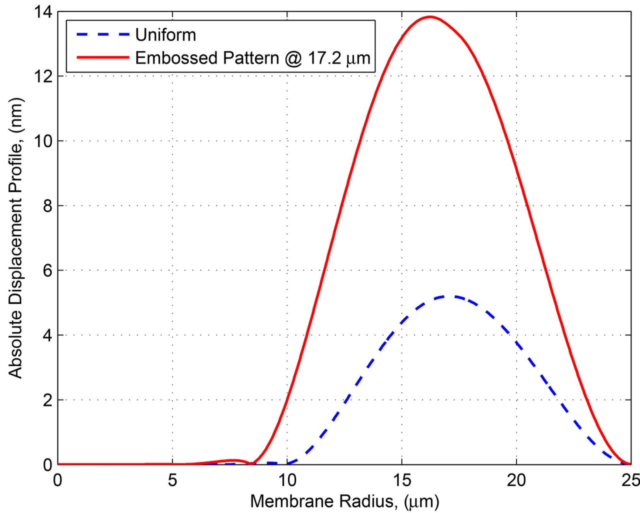

Fig. 6. Dynamic displacement comparison at center frequencies.

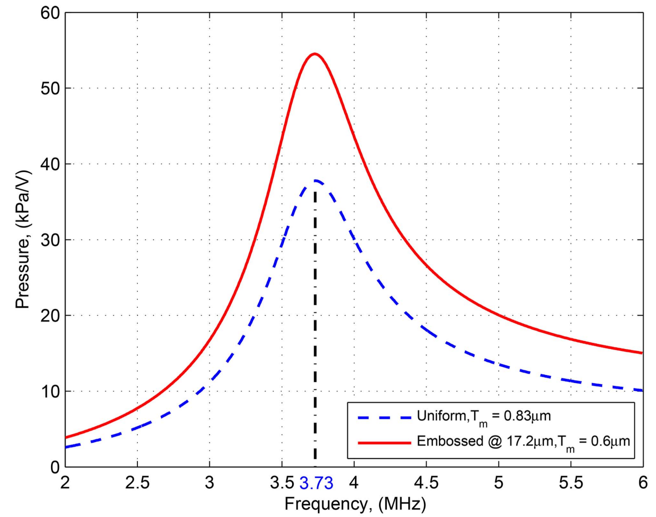

Fig. 8. Thickening uniform membrane to tune center frequency.

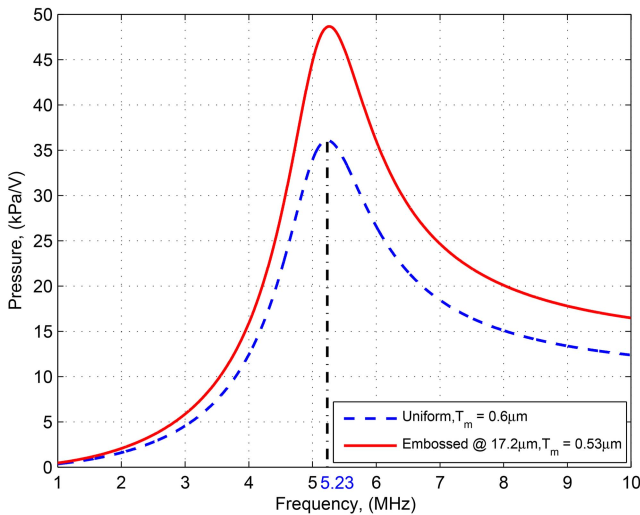

Fig. 7. Thinning embossed membrane to tune center frequency.

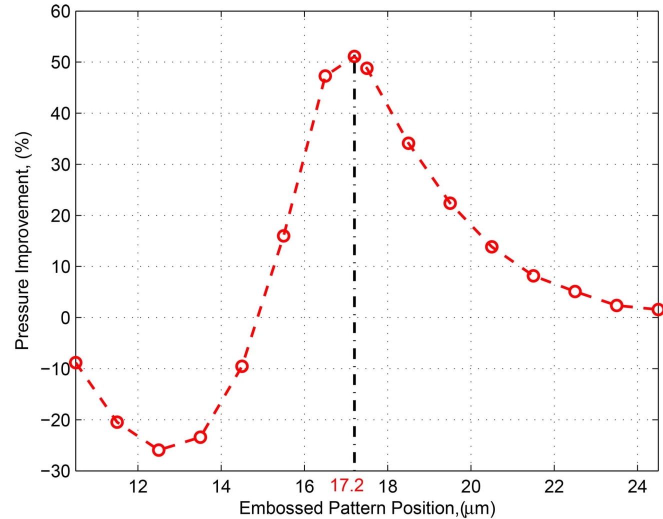

Fig. 9. Maximum output pressure improvement versus the embossed pattern position.

to 5.26 MHz that was similar to the uniform membrane CMUT, by reducing the thickness of the embossed membrane from 0.60 to 0.53 μm. As shown in Fig. 7, the maximum output pressure was improved by 34.9% with the uniform membrane. In the current case, the pressure-bandwidth products of the embossed membrane CMUT and the uniform membrane CMUT were 67.9 and 51.4 kPa MHz, respectively. Alternatively, the center frequency of the uniform membrane CMUT can also be tuned to 3.73 MHz by increasing its membrane thickness from 0.60 to 0.83 μm. As shown in Fig. 8, the improvement of the output pressure by the proposed structure was 44.3%, and the pressure-bandwidth products of the embossed membrane CMUT and the uniform membrane CMUT were 36.2 and 24.6 kPa MHz, respectively.

To investigate the effect to the output pressure caused by the embossed pattern position, the improvement of the maximum output pressure related to the position of the embossed pattern on the vibrating portion without changing the membrane thickness was shown in Fig. 9. Fig. 9 shows that the position of the embossed pattern has a significant influence to the improvement of the maximum output pressure. In extreme cases, e.g., with the position between $r = 10.5$ μm and $r = 14.5$ μm, the embossed pattern has a negative effect to the maximum output pressure. For the embossed pattern located at $r = 12.5$ μm, the output pressure was 25.9% less than that of the uniform membrane model. For the cases of the embossed pattern located at outer portion of the membrane, i.e., $r \geq 22.5$ μm, the improvement of the output pressure was not significant (less than 5%). The simulation results showed that the embossed pattern located near the geometrical center of the vibrating portion of the membrane can achieve higher output pressure. However, the peak output pressure was obtained with the embossed pattern slightly deviated from the geometrical center of the vibrating portion of the membrane. As anticipated by the theoretical derivation with the beam model in Section II, the peak improvement

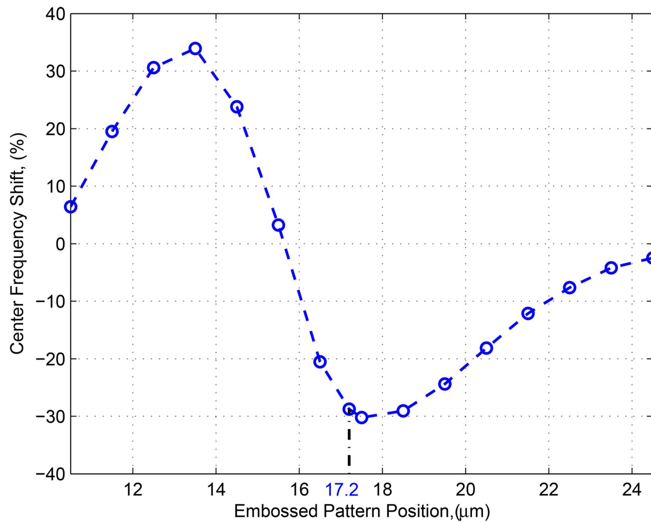

Fig. 10. Relationship of the center frequency shift versus the embossed pattern position.

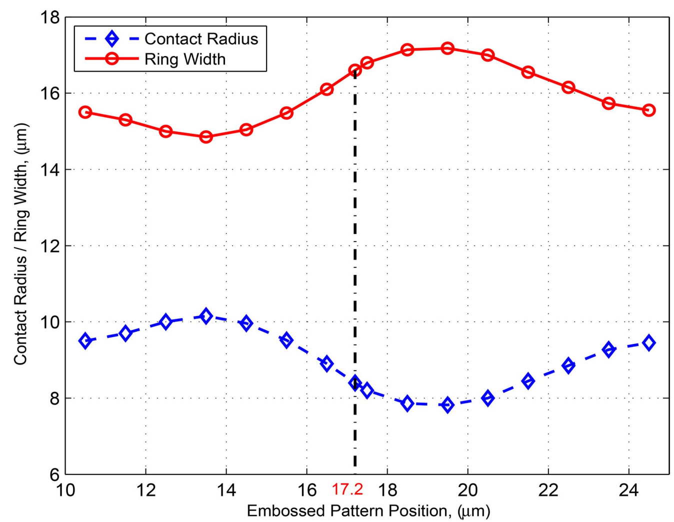

Fig. 11. Embossed pattern position versus contact radius/ring width.

value was obtained when the embossed pattern position was coincided with the location of the maximum deflection ($r = 17.2$ μm), as shown by (7).

B. Center Frequency Shift

For the case of the embossed pattern located at $r = 17.2$ μm, the center frequency shifted down by 28.8%, from 5.23 to 3.73 MHz, as shown in Fig. 5. This frequency shift down phenomenon is anticipated by (16). The percentage of center frequency shift for various positions of the embossed pattern compared with the uniform model is shown in Fig. 10. Similar to the maximum output pressure improvement, the location of the embossed pattern affected the center frequency of the model. The shift of the center frequency ranged from -30.2% to $+33.9\%$. It is found that the position of the embossed pattern was not the sole factor affecting the center frequency shift of the model. From (14), the length of the beam L, which corresponds to the width of the vibrating membrane, is also significant to the center frequency of the model. Because the collapsed membrane contact conditions were not firmly fixed in operation, Fig. 11 shows that the contact radii dependence on the location of the embossed pattern. By comparing Figs. 10 and 11, the trend of the frequency shift was strongly correlated with the width of vibrating membrane.

From Figs. 9 and 10, the simulation results show that the proposed structure has the maximum output pressure improvement when the embossed pattern was located in the vibrating center of the membrane, with the phenomenon of center frequency shift.

As stated, the location of the embossed pattern directly influences the center frequency and the output pressure of the CMUT. In this view, the relationship between the center frequency shift and the output pressure improvement for various embossed pattern locations is shown in Fig. 12, in which the x, y, and z axes refer to pressure improvement,

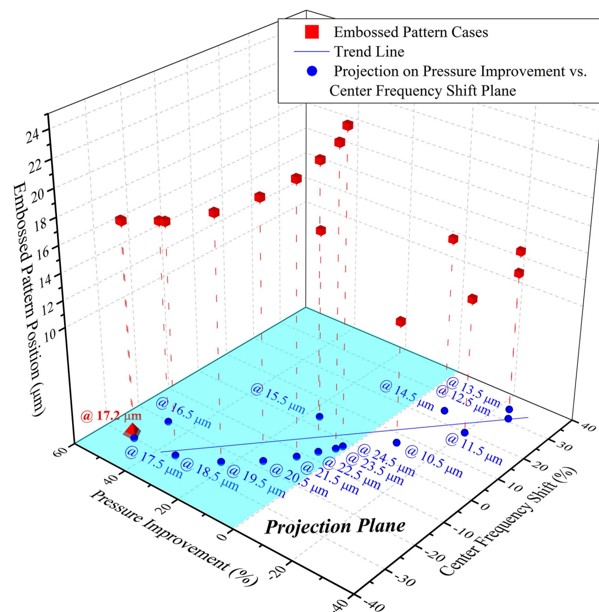

Fig. 12. Relationship between pressure improvement and center frequency shift for various embossed positions.

center frequency shift, and embossed pattern position. As shown, the embossed pattern positions are indicated by red cubes, and the trend line (in blue) on the projection plane suggests that the center frequency shift is inversely proportional to the output pressure improvement. Certainly, the output pressure improvement and the center frequency reach their extreme levels whenever the embossed pattern located at $r = 17.2$ μm and $r = 13.5$ μm, respectively.

Therefore, the location of the embossed pattern inside the shade regions of projection plane can deliver the the reasonable output pressure enhancement, which can be explained further to understand the practical scenario over the membrane due to the embossed pattern by the help of beam model, as mentioned earlier in Section II. Thus, referring to Fig. 2, if the embossed pattern is placed on the vibration center of the membrane,

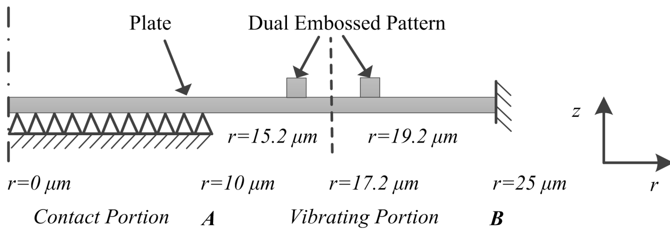

Fig. 13. 2-D axisymmetric view of the dual embossed patterns located symmetrically to the vibrating center.

the output pressure of the proposed CMUT increases; however, the center frequency decreases simultaneously. If the embossed pattern is located away from the vibration center, the center frequency increases, but the output pressure decreases. This is because, the stiffness of the membrane increases with pattern embossment, whereas the overall mass of the membrane changes slightly as the embossed pattern is small. One can observe that the embossed patterns in Fig. 12 residing around the trend line exhibit an asymmetric distribution. This can be attributed by the uneven boundary conditions on the vibrating membrane as the outside perimeter of the membrane is always fixed, whereas the inner one varies due to the change of contact radius in accordance with the pattern embossment.

From the above analysis, the proposed embossed membrane CMUT exhibits a tradeoff relationship with the output pressure and the center frequency. However, as discussed in Section IV-A, the center frequency shift can be compensated by reducing the thickness of the embossed membrane, and the new structure could still achieve 34.9% improvement with a similar center frequency of the uniform membrane CMUT (the center frequency of the new structure CMUT was 5.26 MHz).

C. Further Possible Improvement

The improvement of the maximum output pressure was also evaluated by changing the material of the embossed pattern from PECVD Si_3N_4 to nickel (Ni) that has a higher mass density than silicon nitride. The Ni embossed pattern can be formed on the top aluminum electrode by the sputtering method. In addition to this, a collapse-mode CMUT with dual embossed patterns made of PECVD Si_3N_4 and Ni was simulated as well. Two embossed patterns, each with identical size as in single embossed pattern, were separated by 4 μm symmetrically to the vibrating center of the vibrating portion, as shown in Fig. 13.

Table III shows the improvements in different cases. For case A, the embossed membrane thickness was kept to 0.60 μm, which was the same as the uniform membrane thickness, so their center frequencies were lower than that of the original CMUT. To make a fair comparison, in case B, each embossed membrane thickness was reduced to make the center frequency to be similar to that of the original CMUT. For both dual embossed patterns CMUT and Ni pattern CMUT in all cases, the improvements of the output pressure were higher than that of the single Si_3N_4 pattern, respectively. They are considered to equivalently increase the effective mass of the embossed pattern at the vibrating center, resulting in the improvement of the output pressure.

TABLE III
IMPROVEMENT OF OUTPUT PRESSURE WITH DIFFERENT EMBOSSED PATTERNS

Embossed pattern position	Improvement (%)	
	Case A*	Case B **
Single in vibrating center (Si_3N_4)	+51.1	+34.9
Single in vibrating center (Ni)	+88.1	+46.7
Dual in symmetry (Si_3N_4)	+94.9	+41.3
Dual in symmetry (Ni)	+101.8	+52.0

*The membrane thicknesses of all four cases were the same as the uniform membrane CMUT.
**The membrane thicknesses of all four cases were reduced so as to maintain the the center frequencies of all four cases similar to the uniform membrane CMUT.

V. CONCLUSION

In this paper, an effective method is proposed to improve the maximum output pressure for CMUTs working in the collapse mode. This method, which is compatible with the existing fabrication technology, forms an embossed pattern on the vibrating membrane in order to enhance the energy stored in transmission. Supported with the beam model in undamped conditions and FEA simulation results, the proposed method outperforms the uniform membrane CMUT in terms of output pressure, bandwidth, and, hence, pressure-bandwidth product. In addition, by replacing the embossed pattern with a higher mass density material or dual embossed patterns on the membrane was also investigated and achieved up to 101.8% improvement on the maximum output pressure.

This paper also pointed out that the location of the embossed pattern is crucial to the output pressure improvement and center frequency of the device. However, owing to the nonuniform electrostatic force in the collapse-mode operation, the maximum vibration position is not coincided with the geometrical center of the membrane. Thus, to achieve the highest output pressure improvement, the embossed pattern should be placed at the maximum vibration point on the vibrating membrane, which is estimated by the beam model. The reason is that the embossed pattern can enhance the energy stored in the membrane with the minimum effect on the stiffness of membrane at this position.

However, some issues remain in the future work, for example, the performance of the proposed CMUT is to be experimentally evaluated on a device.

ACKNOWLEDGMENT

The authors would like to thank Y. K. Veng, C. K. Lao, and C. U Kin at the University of Macau and K. K. Park at Hanyang University, South Korea, for the valuable technical support.

REFERENCES

[1] J. A. Jensen, "Medical ultrasound imaging," *Prog. Biophys. Molecular Biol.*, vol. 93, nos. 1–3, pp. 153–165, 2007.
[2] K. Suzuki, K. Higuchi, and H. Tanigawa, "A silicon electrostatic ultrasonic transducer," *IEEE Trans. Ultrason., Ferroelectr., Freq. Control*, vol. 36, no. 6, pp. 620–627, Nov. 1989.
[3] M. Rafiq and C. Wykes, "The performance of capacitive ultrasonic transducers using v-grooved backplates," *Meas. Sci. Technol.*, vol. 2, no. 2, pp. 168–174, 1991.

[4] Ö. Oralkan *et al.*, "Capacitive micromachined ultrasonic transducers: Next-generation arrays for acoustic imaging?" *IEEE Trans. Ultrason., Ferroelectr., Freq. Control*, vol. 49, no. 11, pp. 1596–1610, Nov. 2002.
[5] S. H. Wong, M. Kupnik, R. D. Watkins, K. Butts-Pauly, and B. T. Khuri-Yakub, "Capacitive micromachined ultrasonic transducers for therapeutic ultrasound applications," *IEEE Trans. Biomed. Eng.*, vol. 57, no. 1, pp. 114–123, Jan. 2010.
[6] Ö. Oralkan *et al.*, "Initial pulse-echo imaging results with one-dimensional capacitive micromachined ultrasonic transducer arrays," in *Proc. IEEE Ultrason. Symp.*, Oct. 2000, pp. 959–962.
[7] Ö. Oralkan *et al.*, "Volumetric ultrasound imaging using 2-D CMUT arrays," *IEEE Trans. Ultrason., Ferroelectr., Freq. Control*, vol. 50, no. 11, pp. 1581–1594, Nov. 2003.
[8] D. M. Mills and L. S. Smith, "Real-time *in-vivo* imaging with capacitive micromachined ultrasound transducer (CMUT) linear arrays," in *Proc. IEEE Ultrason. Symp.*, Oct. 2003, pp. 568–571.
[9] B. Bayram, E. Hæggström, G. G. Yaralioglu, and B. T. Khuri-Yakub, "A new regime for operating capacitive micromachined ultrasonic transducers," *IEEE Trans. Ultrason., Ferroelectr., Freq. Control*, vol. 50, no. 9, pp. 1184–1190, Sep. 2003.
[10] Ö. Oralkan *et al.*, "Experimental characterization of collapse-mode CMUT operation," *IEEE Trans. Ultrason., Ferroelect., Freq. Control*, vol. 53, no. 8, pp. 1513–1523, Aug. 2006.
[11] Y. Huang *et al.*, "Comparison of conventional and collapsed region operation of capacitive micromachined ultrasonic transducers," *IEEE Trans. Ultrason., Ferroelectr., Freq. Control*, vol. 53, no. 10, pp. 1918–1933, Oct. 2006.
[12] K. K. Park, Ö. Oralkan, and B. T. Khuri-Yakub, "A comparison between conventional and collapse-mode capacitive micromachined ultrasonic transducers in 10-MHz 1-D arrays," *IEEE Trans. Ultrason., Ferroelectr., Freq. Control*, vol. 60, no. 6, pp. 1245–1255, Jun. 2013.
[13] B. Bayram, Ö. Oralkan, A. S. Ergun, E. Hæggström, G. G. Yaralioglu, and B. T. Khuri-Yakub, "Capacitive micromachined ultrasonic transducer design for high power transmission," *IEEE Trans. Ultrason., Ferroelectr., Freq. Control*, vol. 52, no. 2, pp. 326–339, Feb. 2005.
[14] S. Olcum, F. Y. Yamaner, A. Bozkurt, and A. Atalar, "Deep-collapse operation of capacitive micromachined ultrasonic transducers," *IEEE Trans. Ultrason., Ferroelectr., Freq. Control*, vol. 58, no. 11, pp. 2475–2483, Nov. 2011.
[15] Y. Huang, X. Zhuang, E. O. Hæggström, A. S. Ergun, C.-H. Cheng, and B. T. Khuri-Yakub, "Capacitive micromachined ultrasonic transducers with piston-shaped membranes: Fabrication and experimental characterization," *IEEE Trans. Ultrason. Ferroelectr. Freq. Control*, vol. 56, no. 1, pp. 136–145, Jan. 2009.
[16] M. N. Senlik, S. Olcum, and A. Atalar, "Improved performance of CMUT with nonuniform membranes," in *Proc. IEEE Ultrason. Symp.*, Sep. 2005, pp. 597–600.
[17] H.-S. Yoon *et al.*, "Fabrication of CMUT cells with gold center mass for higher output pressure," in *Proc. 10th Int. Symp. Therapeutic Ultrasound (ISTU)*, 2010, pp. 183–188.
[18] S. Olcum, F. Y. Yamaner, A. Bozkurt, H. Köymen, and A. Atalar, "An equivalent circuit model for transmitting capacitive micromachined ultrasonic transducers in collapse mode," *IEEE Trans. Ultrason., Ferroelectr., Freq. Control*, vol. 58, no. 7, pp. 1468–1477, Jul. 2011.
[19] E. Aydogdu, A. Ozgurluk, A. Atalar, and H. Köymen, "Parametric nonlinear lumped element model for circular CMUTs in collapsed mode," *IEEE Trans. Ultrason. Ferroelectr. Freq. Control*, vol. 61, no. 1, pp. 173–181, Jan. 2014.
[20] J. L. Humar, *Dynamics of Structures*, 3rd ed. Boca Raton, FL, USA: CRC Press, 2012.
[21] J. M. Gere and B. J. Goodno, *Mechanics of Materials*, 8th ed. Stamford, CT, USA: Cengage Learning, 2013.
[22] R. O. Guldiken, J. McLean, and F. Degertekin, "CMUTs with dual electrode structure for improved transmit and receive performance," *IEEE Trans. Ultrason., Ferroelectr., Freq. Control*, vol. 53, no. 2, pp. 483–491, Feb. 2006.
[23] M. A. Crisfield, *Non-Linear Finite Element Analysis of Solids and Structures*. Chichester, U.K.: Wiley, 1991.
[24] G. G. Yaralioglu, A. S. Ergun, and B. T. Khuri-Yakub, "Finite-element analysis of capacitive micromachined ultrasonic transducers," *IEEE Trans. Ultrason., Ferroelectr., Freq. Control*, vol. 52, no. 12, pp. 2185–2198, Dec. 2005.
[25] S. Olcum, M. N. Senlik, and A. Atalar, "Optimization of the gain-bandwidth product of capacitive micromachined ultrasonic transducers," *IEEE Trans. Ultrason., Ferroelectr., Freq. Control*, vol. 52, no. 12, pp. 2211–2219, Dec. 2005.

Yuanyu Yu (S'15) received the B.S. degree in biomedical engineering and the M.S. degree in measuring and testing technologies and instruments from the University of Electronic Science and Technology of China, Chengdu, China, in 2000 and 2005, respectively. He is currently pursuing the Ph.D. degree with the Department of Electrical and Computer Engineering, University of Macau, Macau, China.

He was a System Design Engineer with Actions Semiconductor Company, Ltd., Zhuhai, China, from 2005 to 2010. He has been a Research Fellow with the State Key Laboratory of Analog and Mixed-Signal VLSI, University of Macau, since 2012. His current research interests include design, modeling, and fabrication of capacitive micromachined ultrasonic transducers.

Sio Hang Pun (S'11–A'12–M'12) received the master's degree from the Computer and Electrical Program, University of Porto, Porto, Portugal, in 1999, and the Ph.D. degree in electrical and electronics engineering from the University of Macau, Macau, China, in 2012.

He has been an Assistant Professor with the State Key Laboratory of Analog and Mixed-Signal VLSI, University of Macau, since 2012. His current research interests include biomedical electronic circuits, miniaturized sensors for biomedical applications, and human body communication.

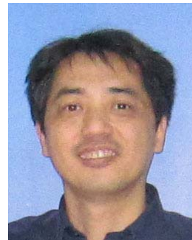

Peng Un Mak (S'88–M'97–SM'11) received the B.Sc. degree from National Taiwan University, Taipei, Taiwan, and the M.Sc. and Ph.D. degrees from Michigan State University, East Lansing, MI, USA, all in electrical engineering.

He has been the first Assistant Professor with the Department of Electrical and Computer Engineering, University of Macau, Macau, China, since 1997. He has authored or co-authored over 140 peer-reviewed technical publications (journal, book chapter, and conference proceedings). His current research interests include biosignals extraction and processing, bioelectromagnetism, human body communication, and body sensor network.

Ching-Hsiang Cheng (M'07) received the B.S. degree in mechanical engineering from National Taiwan University, Taipei, Taiwan, in 1993, three master's degrees in both electrical and mechanical engineering from Cornell University, Ithaca, NY, USA, in 1998, and the Ph.D. degree in electrical engineering from Stanford University, Stanford, CA, USA, in 2005.

He joined Mechanical and Systems Research Laboratories, Industrial Technology Research Institute, Hsinchu, Taiwan, as a Researcher and became a Project Leader, after completing his postdoctoral research with the Department of Mechanical Engineering, Stanford University. In 2006, he was appointed as an Assistant Professor and also a Research Engineer with the Research Institute of Innovative Products and Technologies, The Hong Kong Polytechnic University (PolyU), Hong Kong. In 2010, he joined the Department of Industrial and Systems Engineering, PolyU, as an Assistant Professor. His current research interests include capacitive micromachined ultrasonic transducers, energy storage devices, shear and normal force sensors, large strain and tactile sensors, solar cells, microvalves and micropumps, gas sensors, electrical through-wafer interconnects, nanotechnology, and microelectromechanical systems.

Jiujiang Wang (S'14) received the B.S. degree in microelectronic circuits and systems from the Beijing Institute of Technology, Beijing, China, in 1991, and the M.S. degree in semiconductor devices and microelectronics from the Institute of Semiconductors, Chinese Academy of Sciences, Beijing, in 1994. He is currently pursuing the Ph.D. degree in electrical and computer engineering with the University of Macau, Macau, China.

He was a System Design Engineer in an IC company. His current research interests include modeling and fabrication of capacitive micromachined ultrasonic transducers.

Pui-In Mak (S'00–M'08–SM'11) received the Ph.D. degree from the University of Macau (UM), Macau, China, in 2006.

He is currently an Associate Professor with the Department of Electrical and Computer Engineering, Faculty of Science and Technology, UM, where he is also an Associate Director (Research) of the State Key Laboratory of Analog and Mixed-Signal VLSI. His current research interests include analog and radio-frequency circuits and systems for wireless, biomedical, and physical chemistry applications.

Prof. Mak co-received the DAC/ISSCC Student Paper Award in 2005, the CASS Outstanding Young Author Award in 2010, the SSCS Pre-Doctoral Achievement Awards in 2014 and 2015, the National Scientific and Technological Progress Award in 2011, and the Best Associate Editor of the IEEE TRANSACTIONS ON CIRCUITS AND SYSTEMS—II from 2012 to 2013. In 2005, he was decorated with the Honorary Title of Value for scientific merits by the Macau Government. He was an Editorial Board Member of the *IEEE Press* from 2014 to 2016, an IEEE Distinguished Lecturer from 2014 to 2015, a member of the Board of Governors of the IEEE Circuits and Systems Society from 2009 to 2011, a Senior Editor of the IEEE JOURNAL ON EMERGING AND SELECTED TOPICS IN CIRCUITS AND SYSTEMS from 2014 to 2015, a Guest Editor of the IEEE RFIC VIRTUAL JOURNAL in 2014, and an Associate Editor of the IEEE TRANSACTIONS ON CIRCUITS AND SYSTEMS—I from 2010 to 2011 and from 2014 to 2015, and the IEEE TRANSACTIONS ON CIRCUITS AND SYSTEMS—II from 2010 to 2013. He is the TPC Vice Co-Chair of ASP-DAC'16.

Mang I Vai (M'92–SM'06) received the Ph.D. degree in electrical and electronics engineering from the University of Macau, Macau, China, in 2002.

He has been involved in research in the areas of digital signal processing and embedded systems since 1984. He is currently the Coordinator of the State Key Laboratory of Analog and Mixed-Signal VLSI and an Associate Professor of Electrical and Computer Engineering with the Faculty of Science and Technology, University of Macau.